Reaction Chemistry & Engineering

# Catalytic activity of Pd/hydrophilic phosphine ligand in the interface of an aqueous-phase Cu-free Sonogashira coupling



| | |
|---|---|
| Journal: | *Reaction Chemistry & Engineering* |
| Manuscript ID | RE-ART-02-2018-000021.R1 |
| Article Type: | Paper |
| Date Submitted by the Author: | 09-Mar-2018 |
| Complete List of Authors: | Rizkin, Benjamin; New York University, Department of Chemical and Biomolecular Engineering<br>Hartman, Ryan; New York University, Department of Chemical and Biomolecular Engineering |
| | |

Reaction Chemistry & Engineering

Paper

# Catalytic activity of Pd/ hydrophilic phosphine ligand in the interface of an aqueous-phase Cu-free Sonogashira coupling‡

Received 00th January 20xx,
Accepted 00th January 20xx

DOI: 10.1039/x0xx00000x

www.rsc.org/

Benjamin A. Rizkin and Ryan L. Hartman*[a]

A Cu-free Sonogashira coupling was carried out in a microfluidic reactor with a static organic-aqueous interface and analyzed via in situ Raman spectroscopy. This was the first time that Raman spectroscopy was used in this way to analyze an active cross-coupling. This yielded a better understanding of the reactive interface- mainly that the Pd catalyst is only active in the mixture domain, either the cationic or the anionic deprotonation mechanism describes the reaction, and dissociation of the vinyl-Pd$^{II}$ complex is potentially the rate determining step. The ratio of Pd to hydrophilic ligand is also non-stoichiometric as inactive stable Pd nanoparticles form. This validated previous kinetic models and the assumption that cross-couplings using a hydrophilic ligand can be described by thin film theory. Our findings support that the reaction should be performed with the minimal possible film thickness, which has implications on the design of the reactor. Characterization of the Pd and ligand within the interface is important for deriving accurate kinetic models that maximize catalyst recovery and selectivity while minimizing the environmental impacts of useful compounds when performing green chemistry.

## Introduction

Palladium catalyzed carbon-carbon bond formations are fundamental to modern chemistry. The scale-up and process intensification of cross-couplings are important to green chemistry in fine chemicals, materials, and pharmaceuticals. Over the last two decades investigation of these reactions has formed the basis of three Nobel prizes in Chemistry, but more work is required to understand universal application of homogeneous cross coupling reactions [1]. As an example, the use of hydrophilic ligand in Cu-free Sonogashira couplings‡ further expands the utility of C-C bond formations [2–4]. Through better understanding of the chemistry scientists and engineers will be able to discover economical methodologies to useful compounds where high purity is required and trace catalyst in the product is unacceptable [5,6]. By better understanding the ligand interactions at the aqueous-organic interface using microfluidics with *in situ* Raman spectroscopy we are able to provide a unique perspective on the catalysis.

Cross-coupling catalysis is of broad interest because of the flexibility afforded in the functional groups, allowing a wide range of molecules to be synthesized using very similar chemistry [7]. However, biphasic reactions are complicated and do not have a straight-forward and easily analyzed mechanism with respect to the interactions between the palladium pre-catalyst and ligand, masking the underlying phenomena which lead to reaction rate and mass transfer limitations. Furthermore understanding these phenomena is critical for better analytical modeling of the reaction, producing purer products for the pharmaceutical industry [5,6] and minimizing the environmental metrics (*e.g.*, the E-factor), thereby reducing chemical waste [4].

There are several key advantages to performing the reaction in a two-phase system. First, the precipitation of inorganic salt by-products remains the number one challenge in the field of flow chemistry. Designing hydrophilic ligands for the use of water as a reaction solvent, making the by-products soluble, is one way to overcome this challenge. Second, it becomes much less energy intensive to effectively separate the catalyst. Casalnuovo developed a method of using water-soluble phosphine ligands to ensure that the palladium pre-catalyst remains with the aqueous phase [8]. The organically-soluble catalysts used for these reactions are difficult to separate from the reaction products when the reaction is performed in a single-phase regime, resulting in major difficulties applying this chemistry to regulated industries where trace metals are considered unacceptable, such as pharmaceuticals [5,9]. Thirdly, using a two-phase system with a water-soluble ligand enables recycling of the expensive catalyst [10]. However, varying concentration of the ligand has also been shown to influence mass transfer along with conversion and the E-factor [4]. In process development and intensification it is important to consider atomic economy, yield and volume-time-output criteria along with process robustness and supply chain factors, among others [11,12] and we believe the data presented here will enhance scientists and engineers ability to understand these factors in relevant applications. Finally having a well-mixed system enhances conversion [13], such as in multi-phase flow chemistry [14].

Previous studies of the Pd-catalyzed Sonogashira coupling with hydrophilic phosphines have assumed thin film theory for analysis of the reactive interface, but this was theoretical assumption that had not yet been experimentally validated [2,3].

[a] B. A. Rizkin, Prof. R. L. Hartman
*Department of Chemical and Biomolecular Engineering*
*New York University*
*6 MetroTech Center, Brooklyn, NY (USA)*
*E-mail: ryan.hartman@nyu.edu*

† Footnotes relating to the title and/or authors should appear here.
Electronic Supplementary Information (ESI) available: [details of any supplementary information available should be included here]. See DOI: 10.1039/x0xx00000x

Until now, there was no existing experimental evidence of the direct measurement of Pd or the phosphine ligand at the reacting interface in a liquid-liquid scenario. By using microfluidics with in-situ Raman spectroscopy, better understanding of the interfacial catalysis is possible.

## Results and Discussion

To perform this analysis, we chose the model reaction shown in Scheme 1 [3] because its kinetics were already analyzed [2,4], and all the reagents were readily available in pure form.

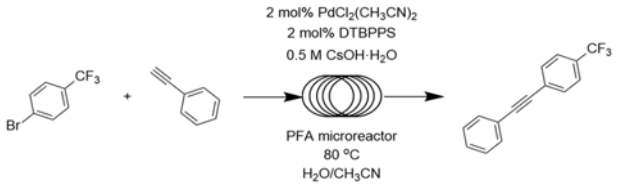


**Scheme 1.** General scheme for the cross-coupling performed. 4-bromobenzotrifluoride was coupled with phenylacetylene using a $PdCl_2(CH_3CN)_2$ pre-catalyst prepared in the organic phase and a DTBPPS ligand in the aqueous phase.

We first performed the reaction in a capillary tube to establish the viability of all the reagents and wet chemistry steps. The conversion was found to be 74.67% (StDev of 2.05%) after one hour, well within the expected range [2,15]. More details of the experimental procedure are provided in the Supporting Information.

To perform the *in-situ* Raman analysis we chose to use a microreactor previously designed [16] due to its ideal chemical, optical, and thermal characteristics for this experiment. The overall geometry of the device is seen in Figure 1A, C and D as consisting of a series of microwells linked via capillaries to the main channel which makes a serpentine around the device. The microwells were initially filled with the aqueous phase *via* capillary forces and then brought in contact with the organic phase *via* flow through the main channel. The aqueous phase formed a bubble inside of each well, which was then surrounded by the organic phase as it flowed in from the main channel, as can be seen in Figure 1C.

Due to the time constraint imposed by probing an active chemical reaction made analyzing the interface quickly using Horiba's SWIFT technology important. An additional complication was the nucleation of vapour bubbles under the beam of the Raman microscope, which was mitigated by applying 0.7 bar backpressure on the system, thus keeping the fluids above their vapour pressure.

To obtain experimental data, a small droplet of water was captured in the microwell and analyzed along its longitudinal axis. A linear map of 1000 points from the upper edge of the top capillary to the bottom edge of the aqueous domain was constructed and spectra were collected in accordance with [16]. The spectra were subsequently deconvoluted to separate the various peaks and then integrated to obtain the relative concentration of each species. An example of a spectrum with its deconvolution is seen in Figure 2A.

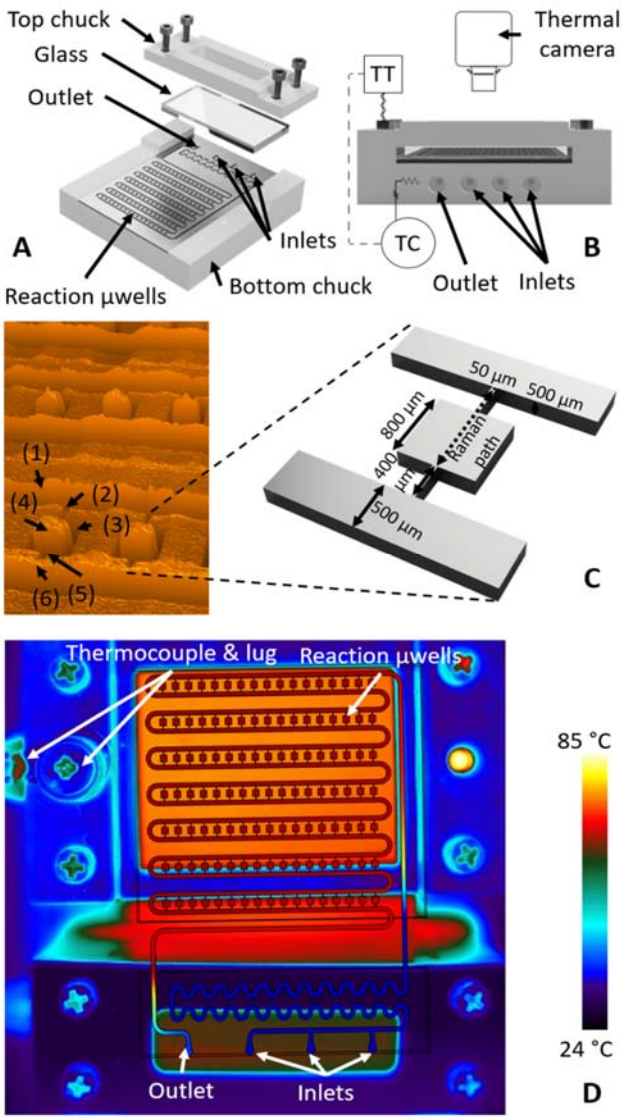


**Figure 1.** (A) CAD rendering of the reactor and chuck assembly. A piece of borosilicate glass is placed between the top of the chuck and reactor to ensure an even distribution of force and prevent cracking the silicon chip. (B) A diagram of the experimental setup used to ensure isothermal operation. (C) An enlarged view the reaction wells filled with aqueous phase. Region (1) denotes the top flow channel, region (2) the top capillary, region (3) the meniscus formed by contact of water to the hydrophobic nitrile, region (4) the water bulk, region (5) the bottom capillary and region (6) the bottom channel. (D) A thermal image of the reactor overlaid with a COMSOL simulation of the same geometry, demonstrating that the reaction is in fact carried out in an isothermal manner.

Once each spectrum was integrated calibration curves were made for each species, using the relative concentration of each species in the bulk hydrophobic and aqueous domains as normalization points. This data was then fit to a Gaussian distribution to mitigate the effects of noise, reflections, differences in refractive indices and other factors from the final data. An example of the raw integration results and the corresponding Gaussian distribution is seen in Figure 2B. In Figure 3 it is observed how the bulk organic phase comes into contact with the aqueous phase at the mixture boundary around 0.32, followed by the mixture zone and then through to

 

the aqueous bulk beginning at about 0.78. Symmetrical behavior is seen on the other side of the interface (Figure 1B).

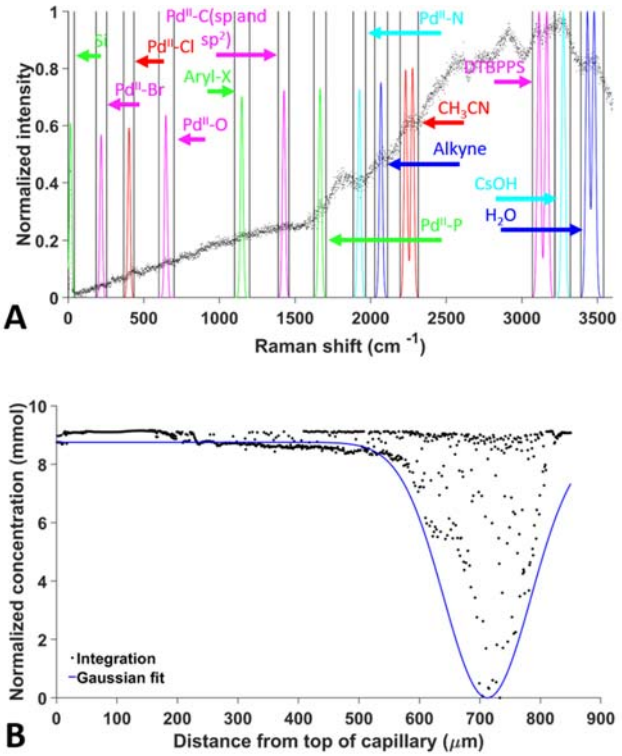


**Figure 2.** (A) A sample Raman spectrum from the reactive interface overlaid with the deconvoluted data from the same spectrum. The reactor materials (Si), ligand (DTBPPS), alkyne (phenylacetylene), 4-bromobenzotrifluoride (Aryl-X), Pd$^{II}$ species, CsOH, $CH_3CN$, and water regions of the spectrum are denoted. (B) As an example, integration results for the alkyne reactant at each point in the Raman scan from bulk hydrophobic through bulk aqueous overlaid with a first order Gaussian fit representing the statistical distribution of reactant molecules in the system.

It was observed in the mixture zone that the concentration of phenylacetylene reaches a minimum at the same point where water reaches its maximum. It can thus be concluded that the bulk of conversion takes place in the mixture domain, with no conversion taking place in the organic or aqueous bulk due to the lack of ligand and consistent alkyne concentration. It is also observed that DTBPPS peaks at the same point as water.

By integrating the total amount of palladium and ligand across the entire system we were able to determine the mole fractions of each species in each phase. This data helped us to determine where in the system the majority of the pre-catalyst and ligand was present, and in what ratios. It was thus found that the mole fraction of Pd$^{II}$-Cl/DTBPPS in the organic phase ($X$) was 0.999/0.0001, the fraction in the interface was 0.673/0.327, and in the aqueous domain it was 0.070/0.930. In Figure 4 it is noted that the ligand reaches its peak mole fraction in the middle of the mixture domain, with a mean value of $6.533 \times 10^{-4}$ versus $3.779 \times 10^{-5}$ in the aqueous bulk. The fraction of Pd pre-catalyst also decreases. These observations support the hypothesis that this is the region of catalytic activity where $PdCl_2(CH_3CN)_2$ is converted to the activated complex $Pd^0L_2$ and the cross-coupling proceeds. Hence, the reaction is only active at the interface between the organic and aqueous phases and nowhere else in the reactor.

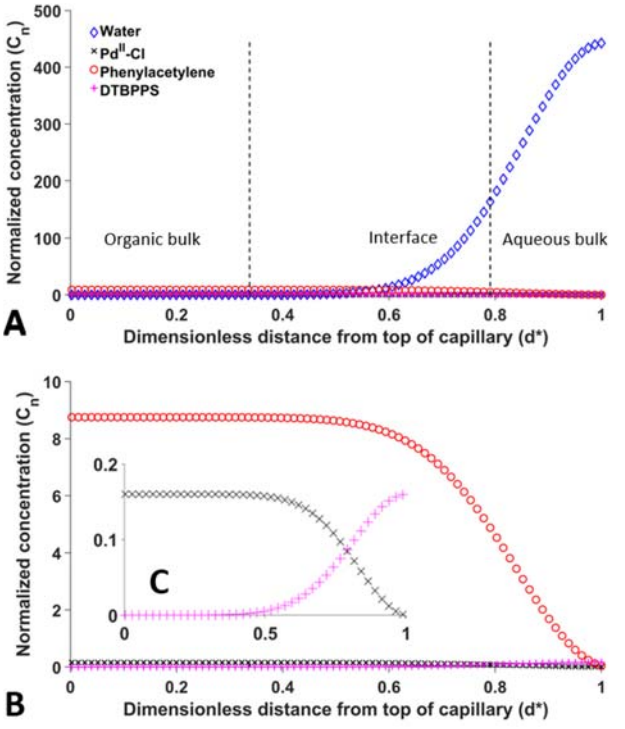


**Figure 3.** (A) Concentration of the various reaction species along the length of the analyzed channel, from organic bulk to aqueous bulk. (B) An enlarged view of the alkyne reactant curve over the same region. (C) An enlarged view of the Pd and ligand concentration curves over the same region.

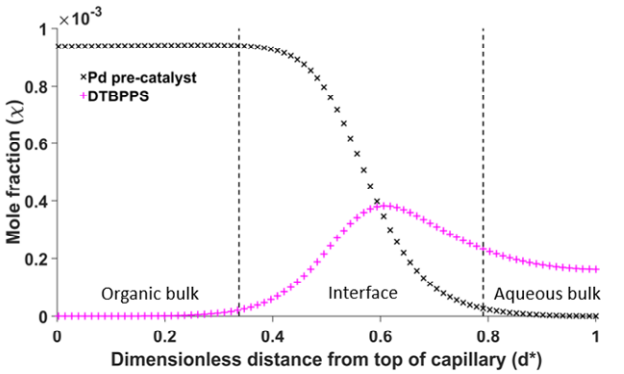


**Figure 4.** Mole fraction curves of the palladium pre-catalyst and ligand computed as the moles of a particular species divided by moles of all analysable species at a particular location. The mole fraction of ligand is highest in the middle of the interface region.

Cationic deprotonation, anionic deprotonation, carbopalladation, and the ionic mechanisms have been proposed for the Cu-free Sonogashira coupling [2-4,17-20], shown in Figure 5. In all mechanisms, the Pd needs to dissociate from a pre-catalyst salt (*e.g.*, from $PdCl_2(CH_3CN)_2$) to bind with two phosphine ligand molecules to begin the catalytic cycle, similar to many C-C bond formations. Only when the palladium atom binds to a minimum of two ligand molecules does it become catalytically active. The catalytic intermediates in either

mechanism, shown schematically in Figure 6, are also exclusive to sp and sp$^2$ carbons bonded with Pd$^{II}$, among Pd$^{II}$-Br.

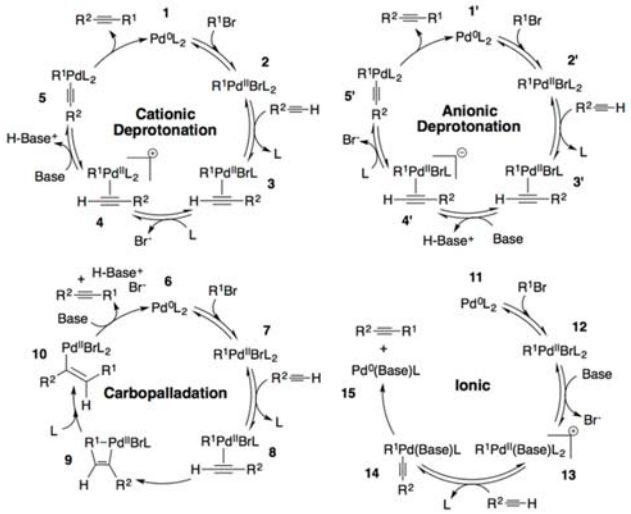


**Figure 5.** Summary of proposed catalytic cycles for the Cu-free Sonogashira coupling: cationic deprotonation, anionic deprotonation, carbopalladation, and the ionic mechanism[2-4,17-20].

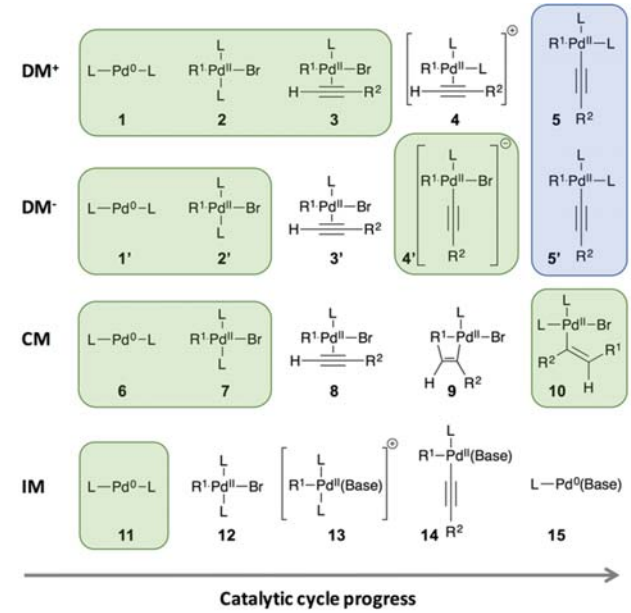


**Figure 6.** Various catalytic intermediates that describe the different proposed reaction mechanisms for the cross-coupling. "DM+" represents the cationic deprotonation mechanism, "DM-" the anionic deprotonation mechanism, "CM" the carbopalladation mechanism, and "IM" is the ionic mechanism. Species highlighted in green are catalytic intermediates that correspond to the largest calculated Gibbs free energy barriers reported for each mechanism using a hydrophilic phosphine [4]. Species highlighted in blue represent the vinyl-Pd$^{II}$ complex, formed in either deprotonation mechanism upon the reductive elimination of the alkyne-Pd$^{II}$ complex (**5** or **5'**).

Palladium itself is known to form stable nanoclusters [21], and Pd black formation is indication the catalyst has deactivated. One would expect, depending on its thermodynamic stability, that Pd nanoparticles could co-exist within the aqueous-organic interface by the formation of Pd-O bonds owing to OH$^-$ nanoparticle surface interactions in the alkaline aqueous media [22,23].

By normalizing the fraction of Pd bond states to the pre-catalyst we were able to isolate the mechanism that governs the cross-coupling. The fraction of Pd$^{II}$-Br bond states in Figure 7 is negligible compared to all other species, which supports that any intermediates with Pd$^{II}$-Br bonds react as fast as they are formed.

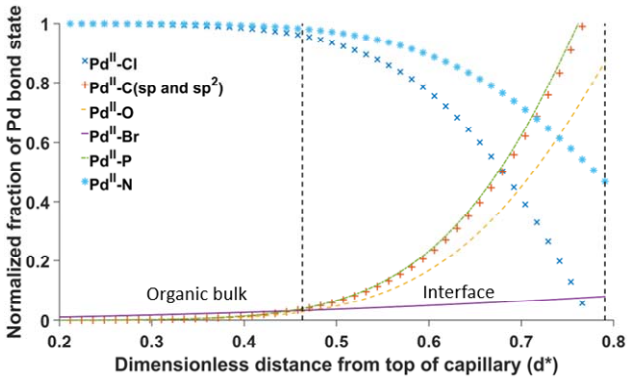


**Figure 7.** Normalized fraction of Pd bond states within the interface. All species were normalized to Pd$^{II}$-Cl. The data illustrates the life-cycle of Pd from the organic bulk through the interface.

This observation rules out **2**, **3**, **2'**, **3'**, **4'**, **7**, **8**, **9**, **10**, and **12** in Figure 6 as precursors to any rate determining steps in their corresponding mechanisms (see Figure 5). Closer inspection of Figure 7 reveals a 1:1 ratio of Pd$^{II}$-C (sp/sp$^2$) to Pd$^{II}$-P bonds, that increases within the interface while the pre-catalyst salt (Pd$^{II}$-Cl and Pd$^{II}$-N) is converted. Thus, oxidative addition of the complex **6** in the carbopalladation mechanism (Figure 5) does not describe the results of Figure 7. Furthermore, replacement of one phosphine in complex **13** with the alkyne (R$^2$-≡-H) to form the alkyne-Pd$^{II}$ complex **14** in the anionic mechanism (see Figure 5) is a barrier-less step [4,18]. With no remaining Pd$^{II}$-C (sp or sp$^2$) bonds in any of the intermediates in Figure 6, the ionic mechanism also does not describe the results of Figure 7.

The vinyl-Pd$^{II}$ complexes (4, **5,** or **5'**), formed in either the cationic or the anionic deprotonation mechanism, are the only activated complexes of any mechanism that have a significant intensity of Pd$^{II}$-C (sp/sp$^2$) and Pd$^{II}$-P bonds (~1:1 ratio). If their intensity ratio corresponds to the stoichiometric molar ratio of those bond states, then product dissociation from the vinyl-Pd$^{II}$ complex is the rate determining step of either cationic or anionic deprotonation catalytic cycle (see Figure 5). Otherwise, oxidative addition could also play a role. In organic solvent with hydrophobic phosphines, oxidative addition of the organohalide to the Pd$^0$L$_2$ complex **1** (or **1'**) in either the deprotonation or the ionic mechanism is thought to control the reaction [18]. The calculated Gibbs free energy barriers for the oxidative addition step and the dissociation of complex **5** (or **5'**) are 97.6 and 86.7 kJ/mol, respectively [4]. A standard deviation of ±10 kJ/mol (due to experimental error) [2,4,18] and the result of Figure 7 suggest that a combination of oxidative addition and product dissociation or product dissociation alone controls either deprotonation mechanism. In any scenario, it is obvious from Figure 7 that the presence of water introduces product dissociation into the rate determining steps of the catalysis,

which could have to do with the fact that the diaryl alkyne product is hydrophobic.

Analysis of the remaining Pd bond states reveals the existence of Pd nanoparticles within the interface. An increasing fraction of $Pd^{II}$-O bonds to the bulk water region, owing to $OH^-$ to Pd nanoparticle surface interactions, indicates deactivation of the catalyst to Pd black. Interestingly, a non-stoichiometric amount of Pd remained bound to N, by a comparison to $Pd^{II}$-Cl bonds. This observation supports that acetonitrile ($Pd^{II}$-$NCCH_3$) could potentially stabilize the Pd nanoparticles as they are formed [22].

One can define the fraction of a catalytic species as F = (moles of the species)/(moles of Pd + moles of DTBPPS) within the interface to better understand the activity. In Figure 8 it is noted that that the molar ratio of Pd to ligand is in favour of Pd in most of the interface until the aqueous boundary.

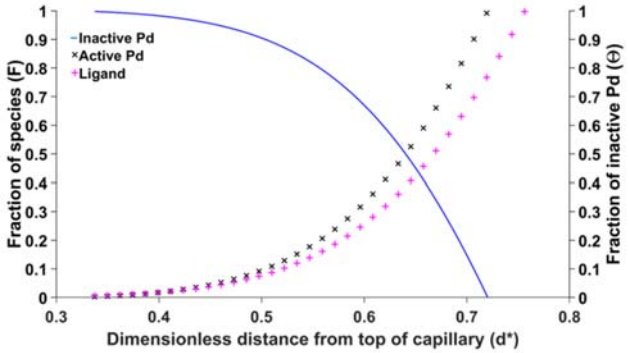


**Figure 8.** Fraction of Pd and ligand species (F) calculated as a fraction of the particular species divided by the sum of all catalytically active species (Pd and ligand) at that point. The secondary y-axis denotes the fraction of Pd in a deactivated state (θ) within the mixture region.

By integrating the normalized concentrations of palladium and ligand within the interface, it is found that the ratio of areas under the two curves is 2.70, which again confirms the existence of inactive Pd.

Analysis of inactive Pd was carried out by defining the fraction of catalytically inactive Pd as $\theta = ([Pd]_i - [DTBPPS]_i/2)/[Pd]_i$ where $i$ is a point within the interface region (see Figure 8) [2]. It is visible that the organic side of the interface nearly all of the Pd pre-catalyst is in the inactive state, whereas the active state is achieved within the interface. Integration under the curves of Figure 8 yields that 47.7 mol% of Pd is inactive within the interface. This suggests the existence of one or multiple phenomenon which is increasing the relative amount of Pd to ligand. The first possibility is mass transfer or thermodynamic limitations resulting from the thickness of the film. The second possibility is the formation of Pd nanoparticles upon deactivation of the active complexes; consistent with the results of Figure 7. Finally, Figure 4 supports that some of the pre-catalyst salt is stable enough in the interface that Pd does not incorporates the ligand, and is thus not catalytically active. These observations undergird that the entire life-cycles of Pd and the ligand should be examined to understand the catalysis.

## Conclusions

Based on the findings presented above it is concluded that the cross-coupling takes place in the mixture region between the organic and aqueous domains since this is the only region with a significant amount of active catalyst. Either the cationic or the anionic deprotonation mechanism describes the cross-coupling, and product dissociation from the vinyl-$Pd^{II}$ complex is possibly the rate determining step of the catalytic cycle. The presence of water influences the rate determining step, likely as a result of the formation of a hydrophobic diaryl alkyne product. The interface also contains inactive Pd in the formation of stable nanoparticles. Due to these phenomenon, the concentration of the ligand in the interface is reduced, thereby decreasing conversion. Therefore, to reach the desired conversion with minimal waste when performing green chemistry, it would be desirable to design ligands with enhanced affinity in the interface or to have a minimally thick film. A way to achieve this would be to ensure an emulsion of the two phases, or reactor designs that minimize the thickness while maximizing the diffusive flux of the catalytic species to and from the interface. It may also be possible to extend the findings of this study to other hydrophilic C-C bond formations for use in new synthetic methodologies or in studies of the catalytic activity.

## Experimental

### Reaction validation

The first phase of the experiment involved preparing and quantifying the reaction in a tubular reactor to verify that the desired levels of conversion were reached. The reactor consisted of several meters of capillary tubing summing up to 0.75 mL in total volume immersed in a stirred oil bath maintained at 80 °C and was performed in accordance with [2]. The aqueous phase consisted of a solution of cesium hydroxide hydrate (base) and 3-(di-tert-butylphosphonium)-propane sulfonate (DTBPPS, ligand) in water. The organic phase consisted of acetonitrile (solvent), 4-bromobenzotrifluoride (halide), phenylacetylene (alkyene), bis(acetonitrile)-dichloropalladium ($PdCl_2(CH_3CN)_2$, Pd pre-catalyst) and mesitylene (GC standard), see Table S1 for more information. Both solutions were prepared inside of a glovebox maintained at <1 PPM O2 and transferred to 10 mL Harvard Apparatus syringes. Water was obtained from a Milli-Q finisher paired with a reverse-osmosis primary purifier, maintained at 18 MΩ/cm final purity. Both phases were mixed using a T-junction and injected into the tubing at a combined flowrate of 180 µL/min into 1/32" IDEX PEEK tubing at various residence times. The reaction product was analyzed with TCD/ FID on an Agilent 7890B.

### Chip preparation

The reactor consisted of an etched silicon chip covered in nitrile that was anodically bonded to a piece of Pyrex® glass [16]. This reactor assembly was clamped in a stainless steel chuck, providing a thermal interface with the resistive heater along

with connections for the various fluid inlets/outlets and thermocouples.

#### Reaction in microfluidic chip

In the second phase of experimentation the interface was analyzed using *in-situ* Raman spectrometry and a novel microfluidic device. This full setup is pictured in the process flow diagram seen in Figure S1 in the supporting information. The chip is composed of a series of 144 microwells in which one phase was confined while the other was flowed through the channels. The system was plumbed with 1/50" PEEK tubing and injection was provided by means of two Harvard Apparatus PHD Ultra 2000 syringe pumps paired with matching 10 mL calibrated syringes. The outlet of the syringe pumps fed into a valve manifold that allows for backwashing of the reactor along with monitoring the pressure *via* McMaster-Carr Standard pressure transducers. The outlet of the valve manifold contained a 2 µm IDEX filter to prevent contamination of the system. Back flow regulation was provided by means of 0.03 bar check valves. A Watlow 100W resistive heater paired with a tuned PID controller provided thermal control of the reaction with an overall accuracy of ±0.2 K.

To perform a trial, the reactor was initially preheated to 80 ºC by means of the resistive heater. The aqueous phase was then injected into the reactor and a slight amount of vacuum followed by back pressure was applied to the outlet to ensure the aqueous phase filled all of the wells via capillary action. Proper filling was analyzed both visually and using Raman spectroscopy. Following the initial filling of the reactor, a secondary injection of the organic phase was performed, which flowed through the channel. By controlling the backpressure carefully, intrusion of the organic phase into the wells could be limited. However, due to the lower surface tension of the organic phase it had a tendency to creep inside the wells via capillary forces and disturb the interface. It was not possible to switch the contents of the well for the organic phase and the channel for the aqueous phase due to precipitation, which would clog the capillaries. Many trials were required to successfully establish an analyzable interface.

After each trials the system was cleaned using toluene and isopropyl alcohol with several hundred reactor volumes being passed through. Passing a stream of dehumidified air through the reactor dried it and prepared it for the next trial.

#### Raman spectroscopy

Raman spectra were acquired using a Horiba LabRam HR evolution with Jobin-Yvon technology paired with a robotic XY stage. Spectra were acquired from 400-4000 $cm^{-1}$ using a 532 nm laser (100% intensity, 6 watts) with a grating of 600 gr·mm-1 and a 1 second acquisition time. A 50x magnification was used along with a CCD Synapse EM detector and Horiba's DualScan and SWIFT technologies. The entire assembly was isolated from vibration on a TMC optical table.

#### Data collection, automation, and analysis

Experimental data collection and pump control were performed through LabVIEW running a combination of code from Harvard Apparatus and proprietary code developed in our lab. Raman spectra were collected in Labspec v6 and analyzed with a combination of Labspec's built-in deconvolution, normalization and baseline correction tools along with MATLAB and GSTools for further analysis and data manipulation. No refraction or reflection pattern corrections were applied, so all data presented here is for apparent concentration only. Peaks of interest were found using a combination of literature [24-27] and the KnowItAll® Informatics System by Bio-Rad Laboratories, Inc. (2017 version) which was used to search the following databases: WSARX, RLS, RZX, RZ2X, RZ3X, FFRX, RHS, RIZ, RJX, RTX, RMX, RGNX, RORX, QRX, QR2X, RAX, RVX, RST1X, RST2X, RST3X, RST4X, RST5X, RST6X and RST7X.

## Conflicts of interest

There are no conflicts to declare.

## Acknowledgements

This material is based upon work supported by the National Science Foundation under Grant Number CBET-1550483. Any opinions, findings, and conclusions or recommendations expressed in this material are those of the authors and do not necessarily reflect the views of the National Science Foundation.

## Notes and references

‡ Note that the name "Sonogashira coupling" is frequently used in the literature with the term "Cu-free". The reaction performed in this study, a Cu-free cross-coupling, is traditionally known as a Heck-Cassar alkyne cross-coupling. The Sonogashira coupling includes a Cu co-catalyst for transmetalation of the alkyne species.

1 C. C. C. Johansson Seechurn, M. O. Kitching, T. J. Colacot, V. Snieckus, *Angew. Chem. Int. Ed.,* 2012, **51**, 5062–5085.
2 J. C. Sabio, R. C. Domier, J. N. Moore, K. H. Shaughnessy, R. L. Hartman, *Chem. Eng. Technol.,* 2015, **38**, 1717–1725.
3 R. C. Domier, J. N. Moore, K. H. Shaughnessy, R. L. Hartman, *Org. Process Res. Dev.,* 2013, **17**, 1262–1271.
4 C. Hu, K. H. Shaughnessy, R. L. Hartman, *React. Chem. Eng.,* 2016, **1**, 65–72.
5 C. E. Garrett, K. Prasad, *Adv. Synth. Catal.,* 2004, **346**, 889–900.
6 J. Magano, J. R. Dunetz, *Chem. Rev.,* 2011, **111**, 2177–2250.
7 K. C. Nicolaou, P. G. Bulger, D. Sarlah, *Angew. Chem. Int. Ed.,* 2005, **44**, 4442–4489.
8 A. L. Casalnuovo, J. C. Calabrese, *J. Am. Chem. Soc.,* 1990, **112**, 4324–4330.
9 C. Torborg, M. Beller, *Adv. Synth. Catal.,* 2009, **351**, 3027–3043.
10 H. Remmele, A. Köllhofer, H. Plenio, *Organometallics*, 2003, **22**, 4098-4103.
11 R. Dach, J. J. Song, F. Roschangar, W. Samstag, C. H. Senanayake, *Org. Process Res. Dev.,* 2012, **16**, 1697–1706.
12 R. B. Leng, M. V. M. Emonds, C. T. Hamilton, J. W. Ringer, *Org. Process Res. Dev.,* 2012, **16**, 415–424.

 

13 J. N. Moore, Synthesis and Application of Sterically Flexible and Water-Soluble Phosphine Ligands in Palladium Catalysis, The University of Alabama, 2014.
14 T. Noël, S. L. Buchwald, *Chem. Soc. Rev.,* 2011, **40**, 5010.
15 S. Ganesamoorthy, K. Shanmugasundaram, R. J. Karvembu, *J. Mol. Catal. A: Chem.,* 2013, **371**, 118–124.
16 B. Pinho, R. L. Hartman, *React. Chem. Eng.,* 2017, **2**, 189–200.
17 T. Ljungdahl, T. Bennur, A. Dallas, H. Emtenäs, J. Mårtensson *Organometallics,* 2008, **27**, 2490−2498.
18 M. Garcia-Melchor, M. C. Pacheco, C. Nájera, A. Lledós, G. Ujaque *ACS Catal.,* 2012, **2**, 135−144.
19 C. Amatore, S. Bensalem, S. Ghalem, A. Jutand, Y. Medjour, *Eur. J. Org. Chem.,* 2004, **2**, 366−371.
20 A. Tougerti, S. Negri, A. Jutand, *Chem. Eur. J.,* 2007, **13**, 666−676.
21 Y. Yang, C. E Castano, B. F. Gupton, A. C. Reberb, S. N. Khanna, *Nanoscale,* 2016, **8**, 19564–19572.
22 X. Yang, M. Zhen, G. Li, X. Liu, X. Wang, C. Shu, L. Jiang, C. Wang, *J. Mater. Chem. A,* 2013, **1**, 8105–8110.
23 F. Kettemann, M. Wuithschick, G. Caputo, R. Kraehnert, N. Pinna, K. Rademann, J. Polte, *CrystEngComm,* 2015, **17**, 1865–1870.
24 W. H. Weber, R. J. Baird and G. W. Graham, *J. Raman Spectrosc.,* 1988**, 19**, 239-244.
25 C. Lu, M. Wang, Z. Feng, Y. Qi, F. Feng, L. Ma, Q. Zhang, X. Li, *Catal. Sci. Technol.,* 2017, **7**, 1581-1589.
26 R. Belka, M. Suchanska, E. Czerwosz, J. Keczkowska, *Cent. Eur. J. Phys.*, 2013, **11**, 245-250
27 M. Capote, G. Papatheodorou, *Inorg. Chem.*, 1978, **12**, 3414-3418

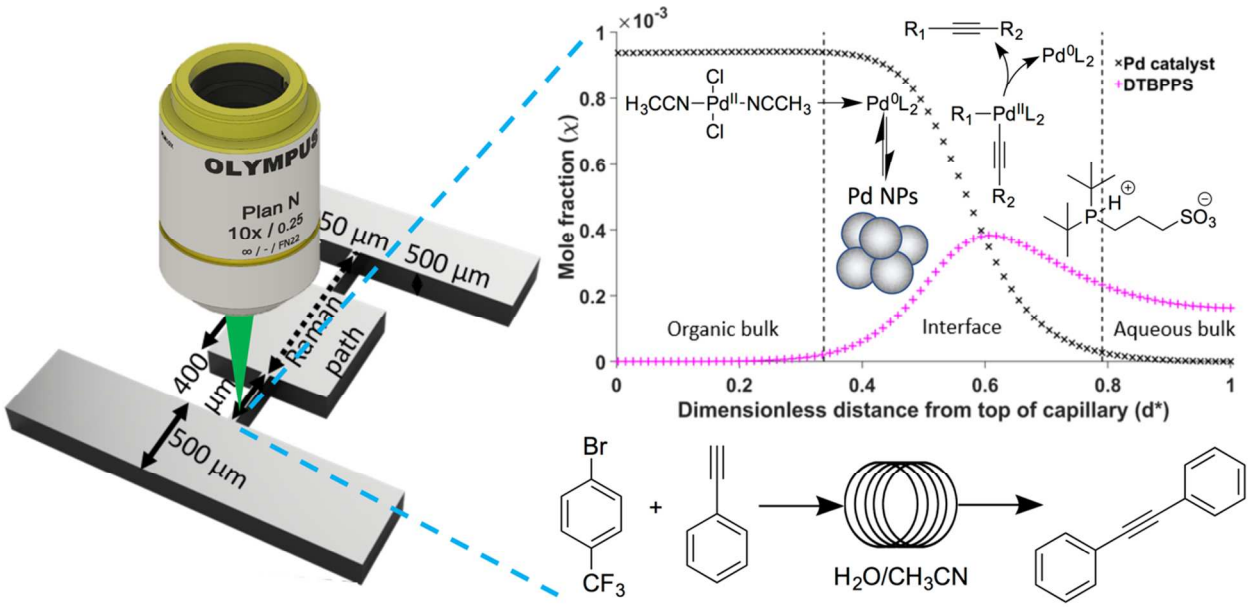


The reaction mechanism and the catalytic lifecycle of a biphasic Sonogashira coupling was studied by microfluidics coupled to Raman spectroscopy.